Photocatalytic Degradation of Methylene Blue *via* Cobalt Doped Fe₃O₄ Nanoparticles

T. Kamakshi[1,2,*,] and G. Sunita Sundari[1]

[1]Department of Physics, Koneru Lakshmaiah Education Foundation, Vaddeswaram-522502, India
[2]Department of Physics, Mallareddy Engineering College for Women, Maisammaguda, Dhulapally, Secunderabad-500014, India

*Corresponding author: E-mail: kamakshi.gopavarapu@gmail.com

Cobalt doped Fe_3O_4 *i.e.*, $CoFe_3O_4$ nanoparticles of different concentrations (0, 0.5, 1.0, 1.5, 2.0, 2.5 mol% were represented as Fe_3O_4, CF1, CF2, CF3, CF4, CF5, respectively) were synthesized using a chemical co-precipitation technique. The XRD patterns and FTIR spectra of Co doped Fe_3O_4 revealed the formation of spinel structure indicating the successful incorporation of cobalt ions with the Fe_3O_4 structure of the iron ions at octahedral sites. Scanning electron micrographs showed a fine uniform spherical particles. UV spectroscopic analysis showed that cobalt doping in $CoFe_3O_4$ nanocomposites influenced the band gap values. These band gap values decreased in the range of 2.76-1.61 eV (direct), 2.53-0.97 eV (indirect) with increase of cobalt content. The activity of $CoFe_3O_4$ in photocatalysis was investigated using methylene blue azo dye under visible light. These results depicted that for 1% cobalt doped Fe_3O_4 novel material photocatalytic activity was enhanced than all other prepared nanomaterials.

Keywords: Fe_3O_4 nanoparticles, $CoFe_3O_4$ nanoparticles, Chemical co-precipitation method, Photocatalysis.

INTRODUCTION

The rapid industrialization (leather, textile, paper, wool, cosmetics) caused water pollution [1] that leads to damage of human health as well as living organisms in water bodies [2,3]. Contaminated water discharging from industries particularly consists of dyes like malachite green, rhodamine B, methylene blue, *etc*. are highly toxic, carcinogenic or mutagenic [4]. These non-biodegradable effluents lead to toxic products; hence their concentration must be reduced to acceptable levels before discharging into environment [5,6]. The removal of toxic effluents from water is a major concern and there are various methods such as chemical precipitation [7], coagulation [8], membrane filtration [9], ion exchange, adsorption [10-12] and photocatalysis [13], *etc*. were used for the elimination of pollutants from contaminated water [4-7,14].

These strategies were doing well only in moving natural compounds from water to another stage. This creates secondary toxic waste that calls for further treatment, which makes the method expensive [15]. Therefore photocatalysis method is widely used due to their low cost, eco-friendliness and is more efficient in treating dyes and ease of processing [16-19]. In

present work, Fe_3O_4 nonmaterial is used, which has a cubic inverse spinel structure, that has engrossed more attention owing to its precise magnetic, biocompatibility and electric properties primarily based on the hopping of electrons among Fe^{2+} and Fe^{3+} ions in the octahedral positions [10]. This material has been utilized in different areas like magnetic resonance imaging [20], catalysts [21], electromagnetic interference shielding materials [22], heavy metals absorbers [23], antibacterial agents [24], in drug delivery systems [25], for direct solar thermal energy harvesting [26], electrochemical biosensors [27]. In nano form, Fe_3O_4 offers increased surface area to volume ratio causing super-paramagnetic behaviour, as a result, improves the decomposition process (by dropping the high surface energy and dipolar attraction of nanoparticles) [11]. Therefore, Fe_3O_4 is considered as one of the important materials for photocatalysis.

Photocatalytic activity has been enhanced by various strategies like doping with transition metals and coupling Fe_3O_4 with other narrow band gap semiconductors [12]. Doping reduces the recombination of charge carriers by transferring them on to the photocatalyst surface [28]. Compared to other magnetic nanomaterials, Fe_3O_4 is the most suitable metal oxide

for photocatalytic degradation of methylene blue because of its highly reactive surface, low toxicity, high electron transport properties, cost efficiency, high adsorption efficiency towards hazardous water pollutant besides facilitate convenient magnetic separation with external magnet for recycling or removal of nanocomposites [29,30]. Though they have superlative properties, there are two major problems arising with Fe_3O_4 nanoparticles. (i) highly prone to agglomeration due to its large surface area, and (ii) because of Fe^{2+} ions present in Fe_3O_4 nonmaterial, these materials easily get oxidized thereby magnetic properties, dispersibility and photocatalytic activity are reduced [31,32].

In order to overcome these problems, studies has been centered on modifying the composition of Fe_3O_4 with doping technique, From literature it is noted that the replacing Fe^{2+} ions with one of a metal ions such as Zn [33], Mn [34], Co [35], Ni [36-38], Ga [39] and Bi [40] will improve physical properties as well as optical properties of Fe_3O_4 originating from electrons hopping between Fe^{2+} and Fe^{3+} ions [41]. Compared to all other transition metals cobalt is more suitable for doping with iron due to its atomic size and better electron valance properties [42]. According to the literature it was found that cobalt dopant is beneficial to separate the charge carriers, improve the recombination lifetime and enhance the efficiency of novel Co doped Fe_3O_4 nanomaterial towards photocatalytic degradation of pollutants in aqueous solution.

Previous literature revealed that a great deal of work has been done using Fe_3O_4 based nanomaterials as photocatalyst in the degradation of different azo dyes. A series of cobalt-doped Fe_3O_4 nano-crystalline particles were successfully prepared in an aqueous solution using the chemical co-precipitation method. Among all, $Co_{0.2}Fe_{2.8}O_4$ nanoparticles exhibited high catalytic efficiency and excellent recyclability in hydrogenation of chloronitrobenzenes (CNBs) to chloroanilines (CAs) at low temperatures in absolute water and at atmospheric pressure [43]. The doping of Co^{2+} could improve the properties of Fe_3O_4 magnetic nanoparticles, *i.e.* enhancing the saturation intensity, decreasing the particle size and making the size distribution homogeneous [44]. The prepared manganese-doped iron oxide (Fe_3O_4) nanoparticles have potential and showed excellent applications for their use in super capacitors [45]. The $LaMnO_3$/Fe_3O_4 with the molar ratio of 1:0.5 showed superior photocatalytic activity [46]. Fe_3O_4/rGO nanocomposite is efficiently utilized towards photocatalytic degradation of carcinogenic and mutagenic cationic as well as anionic dye molecules namely methyl green, methylene blue and rhodamine B under direct sunlight irradiation as an easily recoverable and reusable photocatalyst with potential for many environmental remediation applications [47]. But comparatively less effort has been given towards the degradation of methylene blue dye in industrially contaminated water.

There are no considerable reports of cobalt doped Fe_3O_4 used as a catalyst for degradation of methylene blue in aqueous solution [48]. Hence, present study mainly focused on selective degradation towards methylene blue with in shorter reaction times and high degradation efficiency was achieved without using radical scavengers. It was also observed that cobalt doped Fe_3O_4 provides 87% degradation of methylene blue dye

pollutant in 30 min whereas previous literature reported degradation 78% in 2 h, 87% within 240 min, 35% in 120 min with different methods and combinations [49-51]. Therefore novel optical properties were found in the introduction of Co^{2+} ions by the variation in the band gap of Fe_3O_4, estimated from UV-visible spectrophotometer.

This work deliberates the effect of cobalt doping and its efficiency on photocatalytic degradation of nanoparticles synthesized by chemical co-precipitation method at various doping concentrations of Co^{2+} ions, due to various benefits together with generating adequately water-dispersible nanoparticles in elevated yield, being cost-efficiency, much less instance ingesting, without difficulty scalable for industrial uses and environmentally pleasant [52]. The prepared nanocomposite materials were characterized by XRD, SEM, FTIR spectroscopy and UV-Vis DRS. Degradation of methylene blue dye was monitored using UV-vis spectroscopy. These observations explicate to extent, to which, cobalt doped Fe_3O_4 nanoparticles showed the degradation of irradiated methylene blue through photocatalytic activity. From SEM and UV-Vis DRS characterizations, it was observed that prepared new $CoFe_3O_4$ nanomaterials have porous structure and low energy band gap compared to pure Fe_3O_4, which makes the new $CoFe_3O_4$ nanomaterials are potential candidates for environmental applications [53,54].

EXPERIMENTAL

All the solvents and other reagents, ferrous chloride, cobalt chloride hexahydrate were procured from Sigma Aldrich, while ferric chloride was purchased from Dr. Mac's Bio-pharma Private limited.

Synthesis of $CoFe_3O_4$ nanocomposites: In preparing 0.5% of Co doped Fe_3O_4 nanocomposite, chemical co-precipitation method was used. $FeCl_2 \cdot 4H_2O$ (1.81 g), $CoCl_2 \cdot 6H_2O$ (0.19 g) and $FeCl_3 \cdot 6H_2O$ (5.4 g) were dissolved in 25 mL of dilute HCl solution and then vigorously stirred for 1 h. After that 20.4 mL of NH_4OH solution (about 25% NH_3) was mixed with 225 mL of deionized water. This assortment was immediately added to the initially prepared solution by stirring continuously. Now, this process continued at 80 °C until a light-yellow precipitate was formed, later it turns to black after 0.5 h of stirring. Finally, washed the precipitate with deionized water till the soution becomes netural (pH 7). Dried at 60 °C for 2 h in hot oven to get single phase pure cobalt doped Fe_3O_4 nanoparticles.

Similar procedure has to be continued for other nanocomposites with different concentrations (1 to 2.5%) of cobalt. For the fabrication of pure Fe_3O_4 nanoparticles, the above mentioned technique was maintained with exclusive of using cobalt [55].

Photodegradation technique: Degradation of methylene blue in aqueous solution was evaluated by investigating the catalytic activity of $CoFe_3O_4$ nanoparticles at room temperature under enlightenment of visible light (18 W incandescent bulbs). First 0.1 g of $CoFe_3O_4$ was added to 100 mL of deionized water and then a 10 μL of methylene blue solution was added. This mixture was taken in a beaker (250 mL) and magnetically stirred (120 min) in darkness to obtain adsorption equilibrium between methylene blue dye and $CoFe_3O_4$ nanocomposite. The

TABLE-1
DIFFRACTION ANGLES AND INTENSITIES OF PURE Fe$_3$O$_4$ AND Fe$_3$O$_4$ BASED
NANOCOMPOSITE MATERIALS FROM XRD CHARACTERIZATION

Different planes	Parameters	Samples					
		Fe$_3$O$_4$	CF1	CF2	CF3	CF4	CF5
(220)	Diffraction angle (°)	30.14	30.31	30.27	30.21	30.17	30.15
	Intensity (a.u.)	49.18	361	373	332	299	325
(311)	Diffraction angle (°)	35.4	35.67	35.57	35.58	35.61	35.48
	Intensity (a.u.)	99.5	1034	961	941	972	869
(400)	Diffraction angle (°)	43.16	43.53	43.18	43.26	43.17	43.33
	Intensity (a.u.)	30.07	240	235	187	255	228
(422)	Diffraction angle (°)	53.28	53.82	53.72	54.07	53.81	53.39
	Intensity (a.u.)	19.23	174	149	112	166	106
(511)	Diffraction angle (°)	57.0	57.19	57.36	57.45	57.27	57.2
	Intensity (a.u.)	49.98	308	296	267	352	265
(440)	Diffraction angle (°)	62.68	62.88	62.92	62.69	62.80	62.9
	Intensity (a.u.)	58.89	455	388	357	430	367

resultant solution was kept at 10 cm away from the light source. For every 10 min of irradiation, taken 2 mL solution centrifuged it at 4000 rpm to separate the nanomaterial from solution. The solution equilibrium concentration was investigated by measuring the absorbance at 665 nm (fixed wavelength) using UV-vis spectroscopy [56].

Characterization: The synthesized Fe$_3$O$_4$ based nanocomposites had been analyzed with Bruker AXS D8 Advance diffractometer system, UV-VIS spectrophotometer (Varian, carry 5000) and Thermo Nicolet, Avatar 370 FTIR and F E I Quanta FEG 200-HRSEM to evaluate the structural and optical characteristics.

RESULTS AND DISCUSSION

Fig. 1 shows the diffraction peaks of pure Fe$_3$O$_4$ and cobalt doped Fe$_3$O$_4$ nanoparticles. All these prepared samples showed the reflection peaks at 2θ range of 30.3°, 35.6°, 43.2°, 54.6°, 57.2° and 62.9° corresponding to the planes (2 2 0), (3 1 1), (4 0 0), (4 2 2), (5 1 1) and (4 4 0) indexed as the inverse spinel shape of Fe$_3$O$_4$ (JCPDS: 85-1436). However, the effect of doping shifts the diffraction peaks towards the higher diffraction angle region confirms the formation of CoFe$_3$O$_4$ nanocomposite. It was concluded from Table-1 that with increase in the doping concentrations of cobalt, the increased peak width indicates reduced grain size [57]. The average crystallite size of prepared nanocomposites was determined by observing the maximum intensity peak (311) in XRD pattern using Scherer's formula (D = Kλ/βcos θ) [58,59]. Here K is the Scherrer factor (0.89), λ is the wavelength of incident X-rays (0.15418 nm), β is the FWHM and θ is the Bragg's diffraction angle for the observed peak.

Table-2 shows the average crystallite size of Fe$_3$O$_4$ (pure) and Fe$_3$O$_4$ based nanocomposites and also lattice parameter values. The decreased crystallite size of the cobalt doped Fe$_3$O$_4$ nanoparticles with comparison of pure Fe$_3$O$_4$ nanoparticles represented in Table-2. These are well-matched with the reported values of Rusianto *et al.* [60]. Crystallographic nature of Fe$_3$O$_4$ doesn't change when Fe^{2+} ions replaced by either Co^{2+} or Ni^{2+} ions but its unit cell dimensions [61,62]. Fig. 2 assisted to understand the variation in lattice constant value related to composition. From XRD results, it was concluded that the prepared cobalt doped Fe$_3$O$_4$ nanomaterials exhibited high
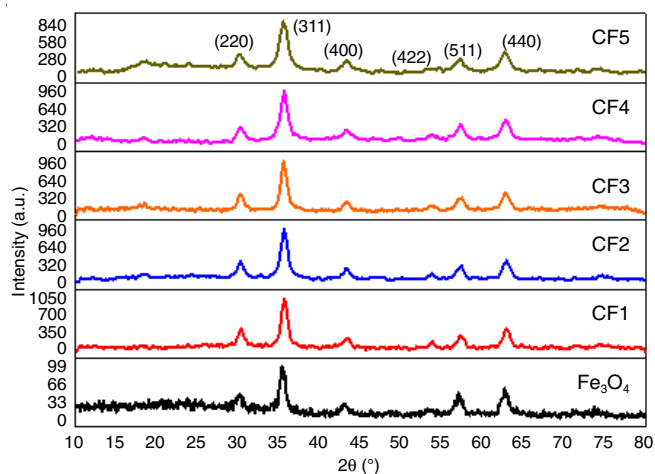
Fig. 1.   XRD patterns of pure Fe$_3$O$_4$ and Fe$_3$O$_4$ based nanocomposite materials: 0.5% cobalt doped Fe$_3$O$_4$ (CF1), 1% cobalt doped Fe$_3$O$_4$ (CF2), 1.5% cobalt doped Fe$_3$O$_4$ (CF3), 2% cobalt doped Fe$_3$O$_4$ (CF4) and 2.5% cobalt doped Fe$_3$O$_4$ (CF5)

TABLE-2
LATTICE CONSTANT OF Fe$_3$O$_4$ (PURE) AND Fe$_3$O$_4$ BASED
NANOCOMPOSITE AND ALSO CRYSTALLITE SIZE OF THE
NANOMATERIALS FROM XRD PEAKS

Sample	Code	d (Å)	a	D = Kλ/βcos θ (nm) for (311)
Fe$_3$O$_4$	Fe$_3$O$_4$	2.522	8.36	11.50
0.5% Co doped Fe$_3$O$_4$	CF1	2.517	8.34	11.20
1.0% Co doped Fe$_3$O$_4$	CF2	2.521	8.35	10.39
1.5% Co doped Fe$_3$O$_4$	CF3	2.520	8.35	11.20
2.0% Co doped Fe$_3$O$_4$	CF4	2.521	8.35	10.39
2.5% Co doped Fe$_3$O$_4$	CF5	2.525	8.37	9.70

D = Average crystallite size calculated from XRD peaks; d = Inter planar distance; a = Lattice constant, a = d$\sqrt{h^2+k^2+l^2}$ degree

crystalline property and cobalt ions successfully incorporated into the Fe$_3$O$_4$ matrix.

Fig. 3 represents the FT-IR spectra of Fe$_3$O$_4$ based nanocomposite materials. The peak observed at around 563 cm^{-1} was attributed to the stretching vibrations of Fe-O bond in tetrahedral region. This peak confirmed the formation of spinel ferrite structure. As the concentration of cobalt doping increased, a peak shifted to a new position at 570 cm^{-1}. This band shift observed was matched with the similar results in the literature.
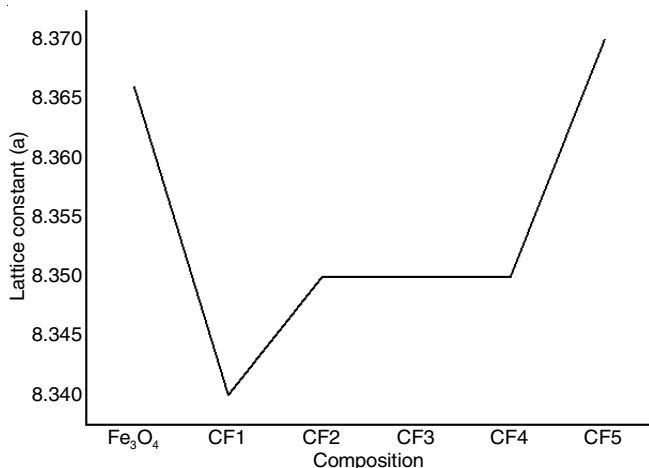
Fig. 2. Variation in lattice constant value related to composition
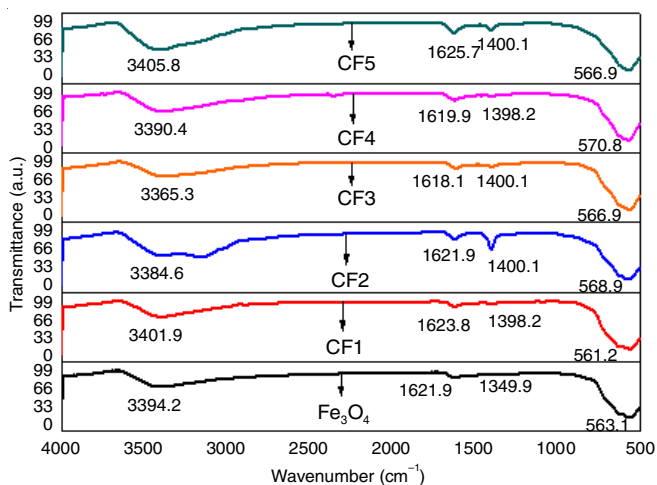
Fig. 3. FTIR spectra of Fe_3O_4 (pure) and 0.5% cobalt doped Fe_3O_4 (CF1), 1% cobalt doped Fe_3O_4 (CF2), 1.5% cobalt doped Fe_3O_4 (CF3), 2% cobalt doped Fe_3O_4 (CF4) and 2.5% cobalt doped Fe_3O_4 (CF5)

The shifting was credited to the change in bond length due to the replacement of Fe^{2+} by Co^{2+} ions in Fe_3O_4 lattice [63]. In 1% of cobalt doped Fe_3O_4 nanomaterial, a strong absorption peak at around 1400 cm^{-1} was also observed, which is a typical FTIR vibrating peak of C=C bond. The presence of peaks at around 1621.9 cm^{-1} was due to C=O bond. Absorption peaks located at around 3394.2 cm^{-1} were due to the stretching vibration of O-H groups [64].

Significantly, these results indicate the presence of both small amounts of water as well as O-H groups on the surface of compound compared to pure and Fe_3O_4 based nanocomposite materials (Table-3). From FTIR results, it was concluded that the prepared cobalt doped Fe_3O_4 nanomaterials had spinel structure and cobalt ions successfully incorporated into the Fe_3O_4 matrix.

SEM images (Fig. 4) identified the presence of voids, pores in cobalt doped Fe_3O_4 based nanocomposite and also agglomerates formed by spherical shaped particles. The reason behind the formation of agglomerates is due to the fact that $CoFe_3O_4$ nanocomposite materials had heavily concentrated nanoparticles owing to its permanent magnetic moment and high surface energy [65,66]. Uniform grains with spherical shaped nanoparticles were observed directly from micrographs, confirmed the crystalline structure of $CoFe_3O_4$. The SEM micrographs of Co-doped Fe_3O_4 confirmed the spherical structure formation and successful doping of Co^{2+} ions into the Fe_3O_4 host structure. SEM characterization results also revealed that porous structure was significant for photocatalytic activity. The particle size of different concentrations of $CoFe_3O_4$ nanomaterials was reduced and comparable with XRD results as shown in Table-4. From SEM results, it is concluded that prepared cobalt doped Fe_3O_4 nanomaterials had pores and small particle size compared to pure Fe_3O_4 nanoparticles. These are the significant characteristics for effective photocatalytic properties [43].
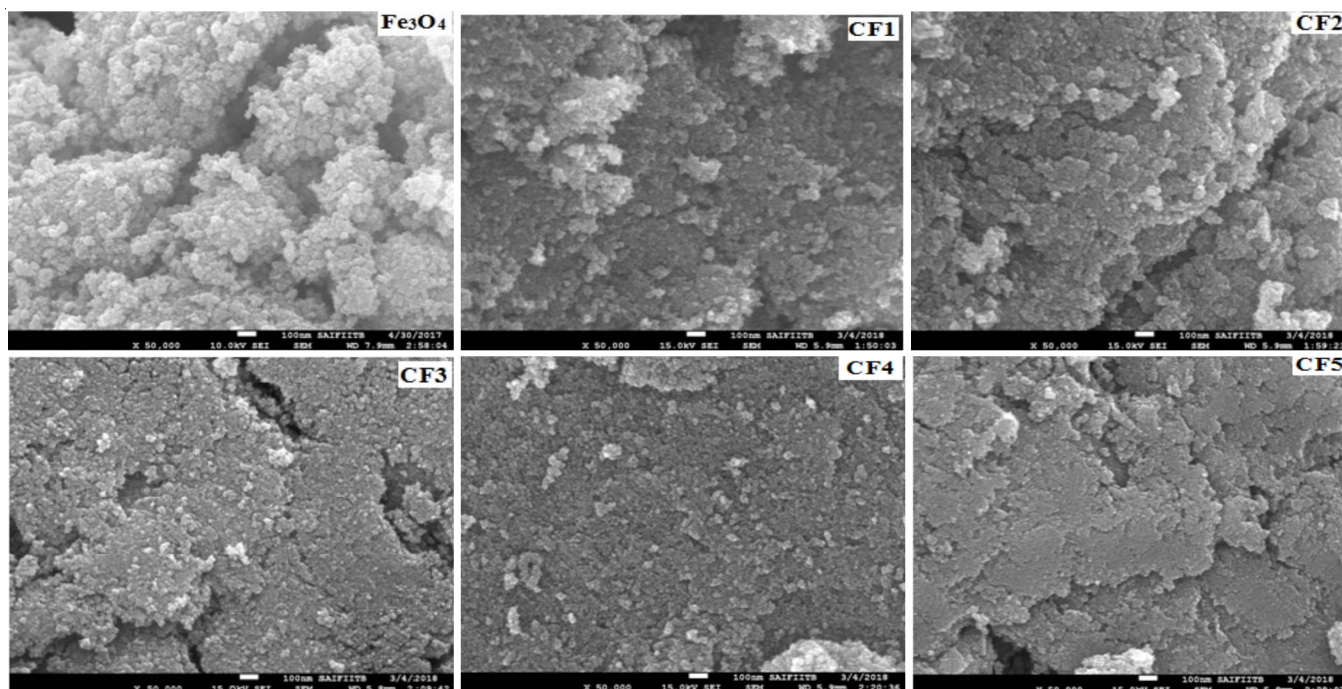
Fig. 4. SEM images of Fe_3O_4 (pure) and 0.5% cobalt doped Fe_3O_4 (CF1), 1% cobalt doped Fe_3O_4 (CF2), 1.5% cobalt doped Fe_3O_4 (CF3), 2% cobalt doped Fe_3O_4 (CF4) and 2.5% cobalt doped Fe_3O_4 (CF5)

TABLE-3
KEY IR BANDS (cm^{-1}) FUNCTIONAL GROUPS OF PURE Fe_3O_4 AND Co-doped Fe_3O_4 (DIFFERENT CONCENTRATIONS)

Type of bon'd	Fe_3O_4	CF1	CF2	CF3	CF4	CF5	Ref.
Stretching vibrations of absorbed hydroxyl groups	3394.2	3390.4	3365.3	3384.6	3401.9	3394.2	[46]
Bending vibrations of absorbed water (H-O-H)	1621.9	1623.8	1621.9	1618.1	1619.9	1625.7	[46]
Deformation of CH_3	1349.9	1398.2	1400.1	1400.1	1398.2	1400.1	[48]
Stretching vibrations of the tetrahedral Fe-O bond	563.1	561.2	568.9	566.9	570.8	566.9	[48]

TABLE-4
COMPARISON TABLE FOR CRYSTALLITE SIZE AND
PARTICLE SIZE OF DIFFERENT CONCENTRATIONS
OF COBALT DOPED Fe_3O_4 NANOPARTICLES

Sample	Code	XRD average crystallite size (nm)	SEM particle size (nm)
Fe_3O_4	Fe_3O_4	11.50	10.13
0.5% Co doped Fe_3O_4	CF1	11.20	10.01
1.0% Co doped Fe_3O_4	CF2	10.39	5.88
1.5% Co doped Fe_3O_4	CF3	11.20	8.89
2.0% Co doped Fe_3O_4	CF4	10.39	5.87
2.5% Co doped Fe_3O_4	CF5	9.70	4.05

TABLE-5
ENERGY BAND GAP VALUES OF
PREPARED NANOMATERIALS

Sample	Code	Band gap values (eV)	
		Direct	Indirect
Fe_3O_4	Fe_3O_4	2.76	2.53
0.5% Co doped Fe_3O_4	CF1	1.71	0.97
1.0% Co doped Fe_3O_4	CF2	1.71	0.97
1.5% Co doped Fe_3O_4	CF3	1.64	0.97
2.0% Co doped Fe_3O_4	CF4	1.63	1.00
2.5% Co doped Fe_3O_4	CF5	1.61	1.00

To study the effect of Co doped Fe_3O_4 nanoparticles on optical band gap; UV-VIS DRS spectra was interned for the wavelength range of 200-800 nm. Fig. 5 showed the light adsorption behaviour of pure Fe_3O_4 and Fe_3O_4 based nanocomposite materials. Electronic transitions in the composite materials lead to light absorption. Light absorptive peak shifted towards the visible region (around 309 to 760 nm) for the cobalt doped Fe_3O_4 nanoparticles compared to pure Fe_3O_4. This was a favourable condition for effective photoactivity. The energy gap values were obtained from Tauc plots for both indirect and direct transitions that were taking place in band gap and band gap values (Table-5). The cause for decrease in the band gap of synthesized nanocomposites was the growth of donor energy levels of transition metal ions. The energy gap contraction was earlier observed in the case of cobalt doped zinc oxide thin films [67] and also in cobalt doped SnO_2 [59]. This can be attributed to the presence of cobalt at Fe^{2+} site in host matrix. However, in the present work, cobalt was predictable to be present at Fe site of Fe_3O_4 lattice, which leads to determine the narrow energy gap. In view of this, presently to conclude that

cobalt ions were integrated within the Fe_3O_4 lattice. This will have an effect on the properties of the semiconductor in terms of band gap.

Diffuse reflectance ultra visible spectra (Fig. 5) were recorded and changed to the Kubelka-Munk function, which is defined [68] as:

$$f_{KM} = \frac{(1-p)^2}{2p} \qquad (1)$$

where p is absolute reflectance.

The band gaps of nanomaterials were observed from Tauc plot. The band gap can be estimated by using eqn. 2:

$$(\alpha h\nu)^n = B(h\nu - E_g) \qquad (2)$$

where B = constant, E_g = energy gap, α = absorption coefficient, h = Planck's constant (6.62×10^{-34} J-s), ν = oscillation frequency and n = constant relating to a mode of transition. Figs. 6 and 7 displayed the E_g values in direct and indirect transition. Direct and indirect energy gap values are reported in Table-5. It was found that when the concentration of cobalt increases, the optical band gap energy decreases.

Fig. 5. UV-visible absorption spectra of Fe_3O_4 (pure) and Fe_3O_4 based nanocomposite materials
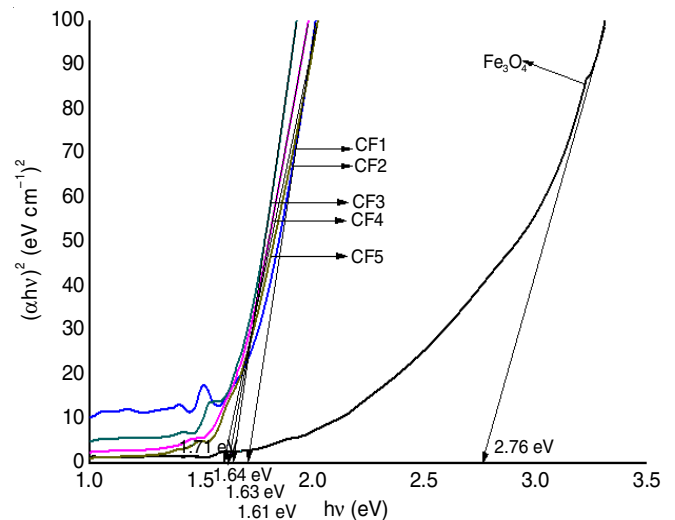
Fig. 6. Tauc plots of pure Fe_3O_4 and Fe_3O_4 based nanocomposite materials for direct band gap energy values
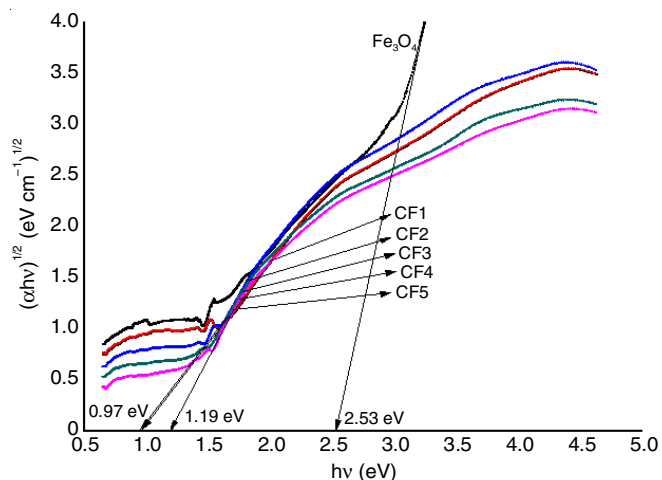
Fig. 7. Tauc plots of pure Fe_3O_4 and Fe_3O_4 based nanocomposite materials for indirect band gap energy values

The photocatalytic activity of pure Fe_3O_4 and Fe_3O_4 based nanocomposite materials were investigated *via* methylene blue degradation. Its general mechanism is shown in Fig. 8. In this process by absorbing visible light energy photogenerated electron-hole pairs were obtained. Consequently, hydroxyl radicals ($^\bullet$OH) produced by the holes react with water (oxidation) and superoxide radicals ($^\bullet O_2^-$) due to the reaction of electrons with oxygen (reduction). These oxidation and reduction mechanisms play a considerable role in the degradation of methylene blue [69-74].
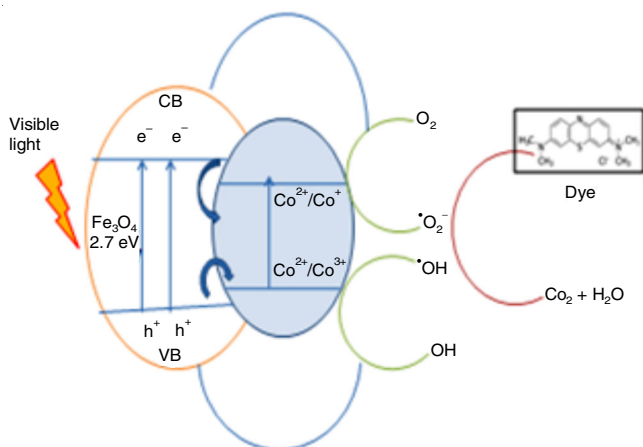
Fig. 8. Schematic representation of photocatalytic activity of $CoFe_3O_4$ nanocomposite materials

Table-6 suggested that cobalt doping increases the photocatalytic activity of $CoFe_3O_4$ up to 1%, hence it was optimized at 1%, beyond this percent catalytic activity reduced. Due to various reasons that were (i) the photogenerated electrons and holes found the more available cobalt ions acted as trap centers; and (ii) cobalt doped nanoparticles might have a tendency to aggregate which leads to decrease number of reactive sites, the light penetration by the suspension and lesser the degradation rate [75-77]. (iii) The effect of cobalt concentration on methylene blue the degradation activity through the photocatalytic process is shown in Fig. 9. Different percentages (0.5-2.5%) of dopant results accelerated degradation efficiency.

TABLE-6
DEGRADATION EFFICIENCY (%) OF
PREPARED NANOCOMPOSITE MATERIALS

Sample	Code	Degradation efficiency (%)
Fe_3O_4	Fe_3O_4	52
0.5% Co doped Fe_3O_4	CF1	74
1.0% Co doped Fe_3O_4	CF2	87
1.5% Co doped Fe_3O_4	CF3	64
2.0% Co doped Fe_3O_4	CF4	75
2.5% Co doped Fe_3O_4	CF5	83
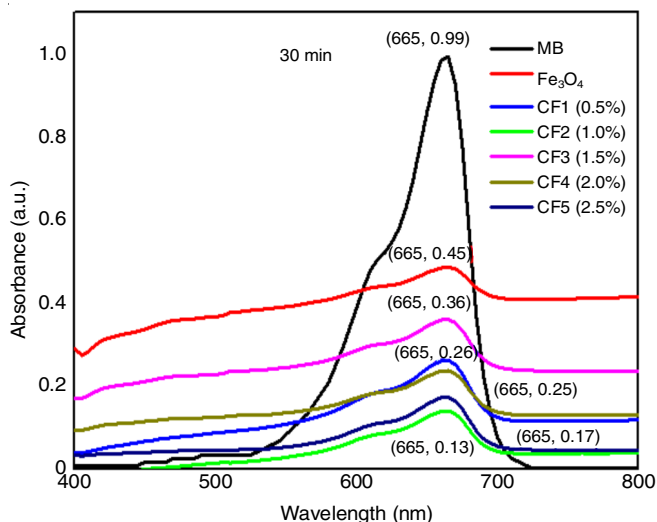
Fig. 9. UV spectra of degradation of methylene blue dye in the presence of Fe_3O_4 (pure) and 0.5% cobalt doped Fe_3O_4 (CF1), 1% cobalt doped Fe_3O_4 (CF2), 1.5% cobalt doped Fe_3O_4 (CF3), 2% cobalt doped Fe_3O_4 (CF4) and 2.5% cobalt doped Fe_3O_4 (CF5)

The degradation efficiency (%) was evaluated from the following eqn. 3 and given in Table-5 [59]:

$$\text{Degradation efficiency (\%)} = \left(1 - \frac{C_t}{C_o}\right) \times 100 \qquad (3)$$

where C_o and C_t are the primary and real-time concentrations of methylene blue, respectively.

Thus, it was concluded that 1% cobalt doped Fe_3O_4 has shown better degradation efficiency compared to pure Fe_3O_4. Also, compared to other works in the literature as shown in Table-7, degradation efficiency of present sample was much better. However, the degradation efficiency was same as compared to the reported 2% cobalt doped CdS [49], but coming to the time frame earlier research has taken 4 h to complete the degradation process, whereas present research showed 0.5 h which is much more acceptable.

Conclusion

Chemical co-precipitation technique was utilized to synthesize pure Fe_3O_4 and Fe_3O_4 based nanocomposite materials. XRD, FTIR, FE-SEM and UV-VIS DRS characterizations established the formation of crystal structure and successful doping of cobalt ions into Fe_3O_4. The photocatalytic activity revealed that 1% of cobalt doped Fe_3O_4 can be considered as potential nanocomposite to degrade methylene blue dye under visible light irradiation relative to pure Fe_3O_4.

TABLE-7
RECENTLY REPORTED PHOTOCATALYTIC SYSTEMS FOR THE
DEGRADATION OF METHYLENE BLUE BY DIFFERENT CATALYSTS

Sample/Source (visible light)	Degradation efficiency	Ref.
FePC/Fe_3O_4 in the presence of H_2O_2	78% in 120 min	[49]
2% Co doped CdS	87% after 240 min irradiation	[50]
1% Co doped $BiFeO_3$	35.06% in 120 min	[51]
Fe_3O_4	52% in 30 min	Present work
1% Co doped Fe_3O_4	87% in 30 min	Present work

CONFLICT OF INTEREST

The authors declare that there is no conflict of interests regarding the publication of this article.

REFERENCES

1. D. Chakraborty and K. Mukhopadhyay, Water Pollution and Abatement Policy in India, A Study from an Economic Perspective; In: Book Series: Global Issues in Water Policy, Springer Netherlands (2014).

2. W. Zhang and C.W. Wu, *Chem. Pap.*, **68**, 330 (2014);
https://doi.org/10.2478/s11696-013-0444-3

3. S. Nagai, *Science*, **130**, 1188 (1959);
https://doi.org/10.1126/science.130.3383.1188-a

4. H. Lin, H. Zhang and L. Hou, *J. Hazard. Mater.*, **276**, 182 (2014);
https://doi.org/10.1016/j.jhazmat.2014.05.021

5. Y.S. Na, C.H. Lee, T.K. Lee, S.W. Lee, Y.S. Park, Y.K. Oh, S.H. Park and S.K. Song, *Korean J. Chem. Eng.*, **22**, 246 (2005);
https://doi.org/10.1007/BF02701492

6. A. Baban, *Clean Soil Air Water*, **41**, 976 (2013);
https://doi.org/10.1002/clen.201200145

7. X. Zhang, M. Lu, M.A. Mohamed Idrus, C. Crombie and J. Veeriah, *Process Safe Environ.*, **126**, 18 (2019);
https://doi.org/10.1016/j.psep.2019.03.024

8. O. Bello, Y. Hamam and K. Djouani, *Alexandria Eng. J.*, **53**, 939 (2014);
https://doi.org/10.1016/j.aej.2014.08.002

9. H.T. Madsen, Membrane Filtration in Water Treatment: Removal of Micropollutants, In: Chemistry of Advanced Environmental Purification Processes of Water, Elsevier Science: Holland, pp. 199-248 (2014).

10. R. Suresh, K. Giribabu, R. Manigandan, L. Vijayalakshmi, A. Stephen and V. Narayanan, *AIP Conf. Proc.*, **1576**, 122 (2014);
https://doi.org/10.1063/1.4861998

11. A.B. Chin and I. Yaacob, *J. Mater. Process. Technol.*, **191**, 235 (2007);
https://doi.org/10.1016/j.jmatprotec.2007.03.011

12. S. Buddee, C. Suwanchawalit and S. Wongnawa, *Dig. J. Nanomater. Biostruct.*, **12**, 829 (2017).

13. Xuan Sang Nguyen, *J. Surf. Eng. Mater. Adv. Technol.*, **8**, 1 (2018).

14. F. Fu and Q. Wang, *J. Environ. Manage.*, **92**, 407 (2011);
https://doi.org/10.1016/j.jenvman.2010.11.011

15. R. Saravanan, F. Gracia and A. Stephen, Basic Principles, Mechanism, and Challenges of Photocatalysis In: Nanocomposites for Visible Light-induced Photocatalysis, Springer International Publishing, Chap. 2 (2017).

16. B. Prasad, C. Ghosh, A. Chakraborty, N. Bandyopadhyay and R.K. Ray, *Desalination*, **274**, 105 (2011);
https://doi.org/10.1016/j.desal.2011.01.081

17. P. Benjwal and K.K. Kar, *J. Environ. Chem. Eng.*, **3**, 2076 (2015);
https://doi.org/10.1016/j.jece.2015.07.009

18. M.J. Allen, V.C. Tung and R.B. Kaner, *Chem. Rev.*, **110**, 132 (2010);
https://doi.org/10.1021/cr900070d

19. A.K. Geim and K.S. Novoselov, *Nat. Mater.*, **6**, 183 (2007);
https://doi.org/10.1038/nmat1849

20. A.H. Rezayan, M. Mousavi, S. Kheirjou, G. Amoabediny, M.S. Ardestani and J. Mohammadnejad, *J. Magn. Mater.*, **420**, 210 (2016);
https://doi.org/10.1016/j.jmmm.2016.07.003

21. M. Arefi, D. Saberi, M. Karimi and A. Heydari, *ACS Comb. Sci.*, **17**, 341 (2015);
https://doi.org/10.1021/co5001844

22. X. Jian, B. Wu, Y. Wei, S.X. Dou, X. Wang, W. He and N. Mahmood, *ACS Appl. Mater. Interfaces*, **8**, 6101 (2016);
https://doi.org/10.1021/acsami.6b00388

23. K. Kalantari, M. Ahmad, H. Masoumi, K. Shameli, M. Basri and R. Khandanlou, *Int. J. Mol. Sci.*, **15**, 12913 (2014);
https://doi.org/10.3390/ijms150712913

24. Y.T. Prabhu, K.V. Rao, B.S. Kumari, V.S.S. Kumar and T. Pavani, *Int. Nano Lett.*, **5**, 85 (2015);
https://doi.org/10.1007/s40089-015-0141-z

25. L.T. Thu Huong, N.H. Nam, D.H. Doan, H.T. My Nhung, B.T. Quang, P.H. Nam, P.Q. Thong, N.X. Phuc and H.P. Thu, *Mater. Chem. Phys.*, **172**, 98 (2016);
https://doi.org/10.1016/j.matchemphys.2015.12.065

26. Y. Chen, X. Quan, Z. Wang, C. Lee, Z.Z. Wang, P. Tao, C. Song, J. Wu, W. Shang and T. Deng, *J. Mater. Chem. A Mater. Energy Sustain.*, **4**, 17503 (2016);
https://doi.org/10.1039/C6TA07773K

27. N. Sanaeifar, M. Rabiee, M. Abdolrahim, M. Tahriri, D. Vashaee and L. Tayebi, *Anal. Biochem.*, **519**, 19 (2017);
https://doi.org/10.1016/j.ab.2016.12.006

28. A. Emanalzahrani, *Asian J. Chem.*, **29**, 2799 (2017);
https://doi.org/10.14233/ajchem.2017.20959

29. P. Mandal and A.P. Chattopadhyay, *Dalton Trans.*, **44**, 11444 (2015);
https://doi.org/10.1039/C5DT01260K

30. C.T. Yavuz, J.T. Mayo, W.W. Yu, A. Prakash, J.C. Falkner, S. Yean, L. Cong, H.J. Shipley, A. Kan, M. Tomson, D. Natelson and V.L. Colvin, *Science*, **314**, 964 (2006);
https://doi.org/10.1126/science.1131475

31. S.A. Kulkarni, P.S. Sawadh and P.K. Palei, *J. Korean Chem. Soc.*, **58**, 100 (2014);
https://doi.org/10.5012/jkcs.2014.58.1.100

32. H. Wei and E. Wang, *Anal. Chem.*, **80**, 2250 (2008);
https://doi.org/10.1021/ac702203f

33. P.M. Anjana, M.R. Bindhu, M. Umadevi and R.B. Rakhi, *J. Mater. Sci. Mater. Electron.*, **29**, 6040 (2018);
https://doi.org/10.1007/s10854-018-8578-2

34. M. O'Hara, J.C. Carter, C.L. Warner, M.G. Warner and R.S. Addleman, *RSC Adv.*, **6**, 105239 (2016);
https://doi.org/10.1039/C6RA22262E

35. X.J. Sun, F.T. Liu and Q.H. Jiang, *Mater. Sci. Forum*, **688**, 364 (2011);
https://doi.org/10.4028/www.scientific.net/MSF.688.364

36. T. Kamakshi, G.S. Sundari, H. Erothu and R.S. Singh, *Rasayan J. Chem.*, **12**, 531 (2019);
https://doi.org/10.31788/RJC.2019.1225054

37. M. Mohapatra, B. Pandey, S. Anand, R.P. Das and H.C. Verma, *J. Magn. Magn. Mater.*, **295**, 44 (2005);
https://doi.org/10.1016/j.jmmm.2004.12.036

38. S. Larumbe, C. Gomez-Polo, J.I. Pérez-Landazábal, A. García-Prieto, J. Alonso, M.L. Fdez-Gubieda, D. Cordero and J. Gómez, *J. Nanosci. Nanotechnol.*, **12**, 2652 (2012);
https://doi.org/10.1166/jnn.2012.5769

39. K. Recko, U. Klekotka, B. Kalska-Szostko, D. Soloviov, D. Satula and J. Waliszewski, *Acta Phys. Pol. A*, **134**, 998 (2018);
https://doi.org/10.12693/APhysPolA.134.998

40. X. Huang, C. Xu, J. Ma and F. Chen, *Adv. Powder Technol.*, **29**, 796 (2018);
https://doi.org/10.1016/j.apt.2017.12.025

41. M. Yousefi and P. Alimard, *Bull. Chem. Soc. Ethiop.*, **27**, 49 (2013);
https://doi.org/10.4314/bcse.v27i1.5

42. R. Amadelli, L. Samiolo, A. Maldotti, A. Molinari, M. Valigi and D. Gazzoli, *Int. J. Photoenergy*, **2008**, 853753 (2008);
https://doi.org/10.1155/2008/853753

43. B. Yang, Q. Zhang, X. Ma, J. Kang, J. Shi and B. Tang, *Nano Res.*, **9**, 1879 (2016);
https://doi.org/10.1007/s12274-016-1080-3

44. X. Sun, F. Liu and Q. Jiang, *Mater. Sci. Forum*, **688**, 364 (2011);
    https://doi.org/10.4028/www.scientific.net/MSF.688.364

45. M. Aghazadeh, I. Karimzadeh, M.R. Ganjali and A. Behzad, *J. Mater. Sci.: Mater Electron.*, **28**, 18121 (2017);
    https://doi.org/10.1007/s10854-017-7757-x

46. Y.D. Susanti, N. Afifah and R. Saleh, *AIP Conf. Proc.*, **1862**, 030039 (2017);
    https://doi.org/10.1063/1.4991143

47. P.K. Boruah, P. Borthakur, G. Darabdhara, C.K. Kamaja, I. Karbhal, M.V. Shelke, P. Phukan, D. Saikia and M.R. Das, *RSC Adv.*, **6**, 11049 (2016);
    https://doi.org/10.1039/C5RA25035H

48. K. Wang, Y. Yang, T.C. Zhang, Y. Liang and Q. Wang, *RSC Adv.*, **9**, 17664 (2019);
    https://doi.org/10.1039/C9RA01671F

49. K. Wang, L. Yu, S. Yin, H. Li and H. Li, *Pure Appl. Chem.*, **81**, 2327 (2009);
    https://doi.org/10.1351/PAC-CON-08-11-23

50. I.F. Ertis and I. Boz, *Modern Res. Catal.*, **6**, 1 (2017);
    https://doi.org/10.4236/mrc.2017.61001

51. A. Paliwal, R. Banu, R. Ameta and S.C. Ameta, *J. Appl. Chem.*, **6**, 967 (2017).

52. H.D. Nguyen, T.D. Nguyen, D.H. Nguyen and P.T. Nguyen, *Adv. Nat. Sci. Nanosci. Nanotechnol.*, **5**, 035017 (2014);
    https://doi.org/10.1088/2043-6262/5/3/035017

53. N.Z. Logar and V. Kaucic, *Acta Chim. Slov.*, **53**, 117 (2006).

54. M.E. Davis, *Nature*, **417**, 813 (2002);
    https://doi.org/10.1038/nature00785

55. G. Viruthagiri and P. Kannan, *J. Mater. Res. Technol.*, **8**, 127 (2019);
    https://doi.org/10.1016/j.jmrt.2017.06.011

56. P.K. Boruah, P. Borthakur, G. Darabdhara, C.K. Kamaja, I. Karbhal, M.V. Shelke, P. Phukan, D. Saikia and M.R. Das, *RSC Adv.*, **6**, 11049 (2016);
    https://doi.org/10.1039/C5RA25035H

57. A. Lassoued, M.S. Lassoued, S. García-Granda, B. Dkhil, S. Ammar and A. Gadri, *J. Mater. Sci. Mater. Electron.*, **29**, 5726 (2018);
    https://doi.org/10.1007/s10854-018-8543-0

58. P. Prasannalakshmi and N. Shanmugam, *Spectrochim. Acta A Mol. Biomol. Spectrosc.*, **175**, 1 (2017);
    https://doi.org/10.1016/j.saa.2016.12.018

59. C.-M. Hung C.-W. Chen, Y.-Z. Jhuang and C.-D. Dong, *J. Adv. Oxid. Technol.*, **19**, 43 (2016);
    https://doi.org/10.1515/jaots-2016-0105

60. T. Rusianto, M. Wazizwildan and K.A. Kusmono, *Indian J. Eng. Mater. Sci.*, **22**, 175 (2015).

61. C.J. Goss, *Phys Chem. Miner.*, **16**, 164 (1988);
    https://doi.org/10.1007/BF00203200

62. M. Lenglet and B. Lefez, *Solid State Commun.*, **98**, 689 (1996);
    https://doi.org/10.1016/0038-1098(96)00109-3

63. Y.F. Chen, C.Y. Lee, M.Y. Yeng and H.T. Chiu, *J. Cryst. Growth*, **247**, 363 (2003);
    https://doi.org/10.1016/S0022-0248(02)01938-3

64. T. Lo'pez, J.A. Moreno, R. Gómez, X. Bokhimi, J.A. Wang, H. Yee-Madeira, G. Pecchi and P. Reyes, *J. Mater. Chem.*, **12**, 714 (2002);
    https://doi.org/10.1039/b105724n

65. T. Tatarchuk, M. Bououdina, W. Macyk, O. Shyichuk, N. Paliychuk, I. Yaremiy, B. Al-Najar and M. Pacia, *Nanoscale Res. Lett.*, **12**, 141 (2017);
    https://doi.org/10.1186/s11671-017-1899-x

66. S. Sagadevana, Z.Z. Chowdhury and R.F. Rafique, *Mater. Res.*, **21**, e20160533 (2018);
    https://doi.org/10.1590/1980-5373-mr-2016-0533

67. R. Kumar, F. Singh, B. Angadi, J.-W. Choi, W.-K. Choi, K. Jeong, J.-H. Song, M.W. Khan, J.P. Srivastava, A. Kumar and R.P. Tandon, *J. Appl. Phys.*, **100**, 113708 (2006);
    https://doi.org/10.1063/1.2399893

68. R. Joyce Stella, G. Thirumala Rao, V. Pushpa Manjari, B. Babu, C. Rama Krishna and R.V.S.S.N. Ravikumar, *J. Alloys Compd.*, **628**, 39 (2015);
    https://doi.org/10.1016/j.jallcom.2014.11.201

69. P. Khemthong, P. Photai and N. Grisdanurak, *Int. J. Hydrogen Energy*, **38**, 15992 (2013);
    https://doi.org/10.1016/j.ijhydene.2013.10.065

70. S. Wei, Y. Chen, Y. Ma and Z. Shao, *J. Mol. Catal. Chem.*, **331**, 112 (2010);
    https://doi.org/10.1016/j.molcata.2010.08.011

71. Y. Leng, W. Wang, L. Zhang, F. Zabihi and Y. Zhao, *J. Supercrit. Fluids*, **91**, 61 (2014);
    https://doi.org/10.1016/j.supflu.2014.04.012

72. J. Han, Y. Liu, N. Singhal, L. Wang and W. Gao, *Chem. Eng. J.*, **213**, 150 (2012);
    https://doi.org/10.1016/j.cej.2012.09.066

73. C.H. Wu and C.L. Chang, *J. Hazard. Mater.*, **128**, 265 (2006);
    https://doi.org/10.1016/j.jhazmat.2005.08.013

74. J. Wang, J. Yang, X. Li, D. Wang, B. Wei, H. Song, X. Li and S. Fu, *Physica E*, **75**, 66 (2016);
    https://doi.org/10.1016/j.physe.2015.08.040

75. A.-W. Xu, Y. Gao and H.-Q. Liu, *J. Catal.*, **207**, 151 (2002);
    https://doi.org/10.1006/jcat.2002.3539

76. S. Yao, S. Song, Z. Shi and S. Wang, *Desalination Water Treat.*, **51**, 7101 (2013);
    https://doi.org/10.1080/19443994.2013.791784

77. X. Yang, W. Chen, J. Huang, Y. Zhou, Y. Zhu and C. Li, *Sci. Rep.*, **5**, 10632 (2015);
    https://doi.org/10.1038/srep10632